Photoactivated p-Doping of Organic Interlayer Enables Efficient Perovskite/Silicon Tandem Solar Cells

Xiaopeng Zheng, [1,5] ‖ Jiang Liu,[2‖] Tuo Liu,[4‖] Erkan Aydin,[2‖] Min Chen,[5] Wenbo Yan,[2] Michele De Bastiani,[2,8] Thomas G. Allen,[2] Shuai Yuan,[6] Ahmad R. Kirmani,[5] Kyle N. Baustert,[4] Michael F. Salvador,[2] Bekir Turedi,[1] Abdullah Y. Alsalloum,[1] Khulud Almasabi,[1] Konstantinos Kotsovos,[3] Issam Gereige,[3] Liang-Sheng Liao,[6] Joseph M. Luther,[5] Kenneth R. Graham,[4] Omar F. Mohammed,[1,7*] Stefaan De Wolf,[2*] and Osman M. Bakr[1*]

[1]Division of Physical Sciences and Engineering, Catalysis Center (KCC), King Abdullah University of Science and Technology (KAUST), Thuwal 23955-6900, Kingdom of Saudi Arabia

[2]KAUST Solar Center (KSC), Division of Physical Sciences and Engineering, King Abdullah University of Science and Technology (KAUST), Thuwal 23955-6900, Kingdom of Saudi Arabia

3Saudi Aramco Research & Development Center, Dhahran 31311, Kingdom of Saudi Arabia

[4]Department of Chemistry, University of Kentucky, Lexington, Kentucky 40506, United States

[5]National Renewable Energy Laboratory, Golden, Colorado 80401, United States

[6]Jiangsu Key Laboratory for Carbon-Based Functional Materials & Devices, Institute of Functional Nano & Soft Materials (FUNSOM) & Collaborative Innovation Center of Suzhou Nano Science and Technology, Soochow University, Suzhou 215123, China

[7]Division of Physical Sciences and Engineering, Advanced Membranes and Porous Materials Center (AMPM), King Abdullah University of Science and Technology (KAUST), Thuwal 23955-6900, Kingdom of Saudi Arabia

[8]Department of Chemistry & INSTM, Università di Pavia, Via T. Taramelli 14, Pavia 27100, Italy

ABSTRACT: Solution-processed organic semiconductor layers on rough surfaces tend to vary widely in thickness, significantly hindering charge extraction in relevant optoelectronic devices. Here, we report the photoactivated p-doping of hole-transporting material (HTM) to enhance hole extraction for (textured) perovskite/silicon tandem solar cells, making the device performance less sensitive to the variation of hole transport layer thickness. We used the ionic compound 4-isopropyl-4'-methyldiphenyliodonium tetrakis-(penta-fluorophenyl-borate) (DPI-TPFB) as a p-type dopant in poly(triaryl amine) (PTAA), which we used as the HTM. We observed that light soaking DPI-TPFB-doped PTAA shows approximately 22 times higher conductivity compared with an undoped PTAA film, which translated into an improved fill factor (FF) for tandem solar cells. Our tandem solar cells achieved an ~80% FF and 27.8% efficiency; and operated at their maximum power point for 200 h without loss of performance, in addition to retaining ~83% of initial performance over a month of operation in outdoor environment.

Metal halide perovskites (MPs) have attracted extensive attention due to their excellent performance in photovoltaics.[1-7] From 2009 to 2022, the power conversion efficiency (PCE) of single-junction perovskite solar cells (PSCs) jumped from 3.8% to 25.7%.[1, 8-11] This rapid increase in single-junction cell PCE has also spurred increasing attention to develop tandem solar cells that combine low-cost and highly efficient PSCs with lower-band-gap materials, such as crystalline silicon (c-Si) and copper indium gallium selenide (CIGS), to achieve a much higher performance than what could be realized by just a single-junction cell of any of those technologies.[12-23]

Perovskite/silicon tandem cells have been primarily fabricated on single-side-polished silicon bottom subcells.[24-26] Yet, while polished surfaces facilitate perovskite film deposition, they impede photocurrent generation due to undesirable surface reflection. Moreover, double-side-textured c-Si wafers (etched in alkaline solutions) are more industrially relevant and thus promising for use as bottom subcells. Previously reported studies verified the minimized reflection and enhanced spectral utilization with textured tandems.[13, 27-31]

However, textured c-Si wafers are rough – typically covered with random pyramids measuring 1-10 μm on both wafer sides[32]– which makes them challenging substrates for fabricating solution-processed conformal films. In particular, solution-processed organic charge transport layers vary widely in thickness when deposited onto textured surfaces. For example, hole transport layers (HTLs) on textured silicon are much thicker in the valleys than on the pyramid facets.[29]

Such non-uniform HTLs are detrimental to the efficiency of the hole extraction and reduce the fill factor (FF) of devices due to increased series resistance.

By improving hole transport and extraction through chemical doping, devices may be made efficient and less influenced by variations in HTL thickness. For example, Yang et al. reported the use of doped PTAA in perovskite/CIGS tandem cells, which made device performance less sensitive to HTL thickness.[15]

Here, we report a photoactivated p-doped HTL to enhance hole extraction on textured silicon, achieving ~80% FF and ~27.8% PCE for perovskite/silicon tandem solar cells. This p-type doping is activated by a light-soaking treatment which resulted in approximately 22 times higher conductivity compared with an undoped PTAA film, enhancing the performance in perovskite/silicon tandem cells. The corresponding devices also showed no efficiency loss after a 200 h operational stability test under 1-sun illumination and retained ~83% of initial performance after a month of operating in a hot and humid outdoor environment.

Aiming to reduce the dependence of device performance on HTL thickness, we chose the ionic compound 4-isopropyl-4'-methyldiphenyliodonium tetrakis-(penta-fluorophenyl-borate) (DPI-TPFB) as a p-type dopant in a poly(triaryl amine) (PTAA) hole transport material solution in toluene (Figure 1a).[15, 33] Approximately 10 wt% of DPI-TPFB dopant was mixed with PTAA powder to produce a 2 mg/mL PTAA solution in toluene. The color of the doped PTAA solution gradually turned pink under room-light soaking, whereas there was no color change in the dark (Figure 1b inset). We observed strong polaron absorption peaks centered at approximately 500 nm and a monotonic increase in polaron absorption in the 800-1600 nm region corresponding to the oxidized states of PTAA. We also observed photoluminescence (PL) quenching after adding the dopant (Figure 1c), which was more pronounced for the light-soaked doped PTAA (LS-doped PTAA) due to polaron-induced exciton quenching.[34] Electron paramagnetic resonance (EPR) spectroscopy showed a distinct peak for the LS-doped PTAA, whereas no peak was observed for the doped PTAA in the dark (D-doped PTAA) (Figure 1d); this finding indicates that the formation of free radicals requires the participation of light, which promotes the doping of PTAA.[35]

To further explore the electronic properties of doped PTAA, we prepared 100 nm thick PTAA films and carried out conductivity tests via *I-V* analysis on an ITO/PTAA/MoO_3/Al device, as shown in Figure 1e. Because the EPR spectra presented an increased concentration of unpaired electrons, the conductivity of LS-doped PTAA should be higher than that of pristine PTAA and D-doped PTAA. Not surprisingly, as summarized in Table S1, the conductivity jumped from 9.8×10^{-8} S/cm for pristine PTAA to 1.2×10^{-6} S/cm and 2.18×10^{-6} S/cm for D-doped-PTAA and LS-doped-PTAA, respectively. Taken together, these results suggest that light-soaking treatment provides more free charge carriers in DPI-TPFB-doped PTAA.

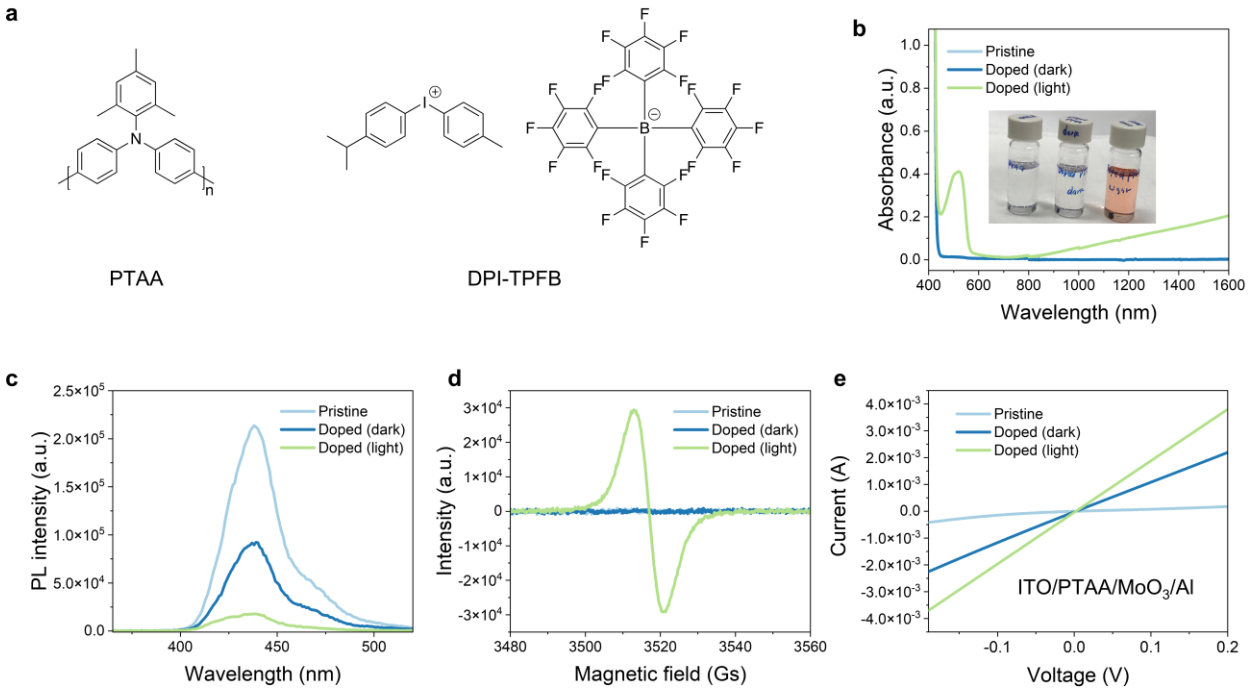

Figure 1. (a) Chemical structures of PTAA and DPI-TPFB. (b) UV-Vis-NRI absorption, (c) PL, and (d) EPR spectra of pristine PTAA and DPI-TPFB-doped PTAA solutions in the dark and under illumination. The inset in (b) is a photograph of the corresponding PTAA solutions. (e) Conductivities of PTAA films in the linear region from -0.2 V to 0.2 V.

Ultraviolet photoelectron spectroscopy (UPS) measurements (Figure S1) were conducted to verify the p-type doping. Figure S1b reveals that the highest occupied molecular orbital (HOMO) onsets of D-doped and LS-doped PTAA are closer to the corresponding Fermi levels than the pure PTAA control, indicating p-type doping. As previously demonstrated, light-soaking treatment activates the doping process in PTAA solutions. Similarly, the ultraviolet (UV) beam used in UPS also likely activated the doping of the D-doped solid-state PTAA film. Photoactivated p-type doping of the D-doped PTAA occurred within a short period, as no shifting was observed in the HOMO region—even when samples were measured with a reduced UV excitation flux and a faster scanning rate. The work functions (WFs) of the D-doped and LS-doped PTAA films are *ca.* 4.9 eV, whereas the WF of the pristine PTAA film is only 4.7 eV, which further supports p-type doping (Figure S1a).

To further elucidate the doping mechanism, we also tried to dope Na tetrakis-(penta-fluorophenyl-borate) (NaTPFB), which shares the same anion with DPI-TPFB, into a PTAA solution with light exposure. The NaTPFB/PTAA solution showed no color change, indicating that the doping effect is mainly stemming from the cation part of the molecule – i.e, DPI. Photolysis of DPI salts has been investigated thoroughly in cationic photopolymerization.[36-37] Herein, we discussed the possible photoactivated doping route in Scheme 1. Based on the previous work reported by J. Dektar *et al.*, DPI cations are likely to undergo direct photolysis by UV irradiation.[36] A neutral phenyl radical and a phenyliodonium cation radical are formed via a homolytic pathway, and a heterolytic cleavage leads to iodobenzene and a phenyl cation. Density functional theory (DFT) calculations made by H. Seim *et al.* indicate that both the phenyliodonium cation radical from the homolytic pathway and phenyl cation from the heterolytic pathway are strong oxidants and able to induce the doping process. Either possible doping route requires light activation, in agreement with the gradual color change of the doped-PTAA solution under light soaking.

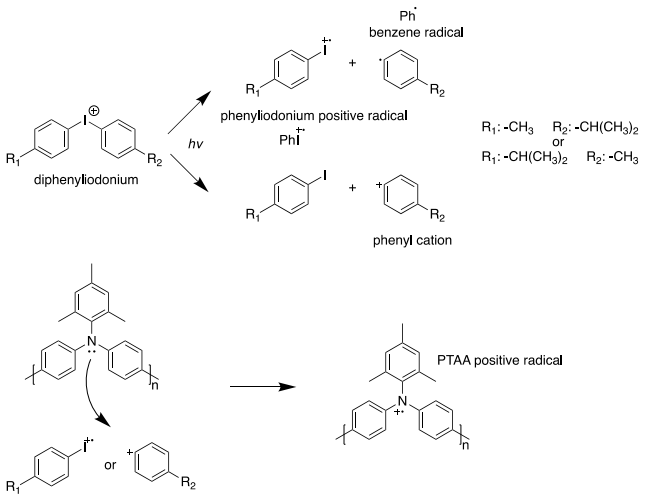

Scheme 1. The possible photolytic PTAA doping process with DPI-TPFB under light soaking.

To exploit the advantages of DPI-TPFB-doped PTAA as an HTL, we fabricated perovskite/silicon tandem cells with the device architecture presented in Figure 2a. The PTAA and perovskite layers were spin-coated on double-side-textured silicon heterojunction (SHJ) bottom cells. The typical silicon bottom cell has a PCE of 19.8%, with a short circuit current density (J_{SC}) of 36.1 mA/cm^2, an open-circuit voltage (V_{OC}) of 0.712 V, an FF of 77% (Figure S2). As shown in the cross-section scanning electron microscopy (SEM) image in Figure 2b, on the roughly textured silicon wafer, the perovskite layer is thick enough to bury the underlying pyramids, as well as planarize the textured silicon bottom cell, preventing the pyramids from protruding. For efficient charge transport, the PTAA layers should be as thin as possible while still uniformly covering the ITO. However, the spin-coated PTAA film accumulates in the valleys to become much thicker in the valleys than that on the facets of pyramids, as clearly shown in Figure 2c. Previous studies have shown that a thick non-doped PTAA layer measuring more than 15 nm reduces the fill factor due to inadequate hole transport.[29] No significant reduction in PTAA thickness in the valleys was observed with the doped PTAA. The X-ray diffraction (XRD) data, as shown in Figure S3, indicate the promotion of (100) for the perovskite film on doped PTAA, which has been shown to help reduce the trap density of the perovskite film.[9] There are no visually apparent morphological changes in the film as shown in the SEM images (Figure S4).

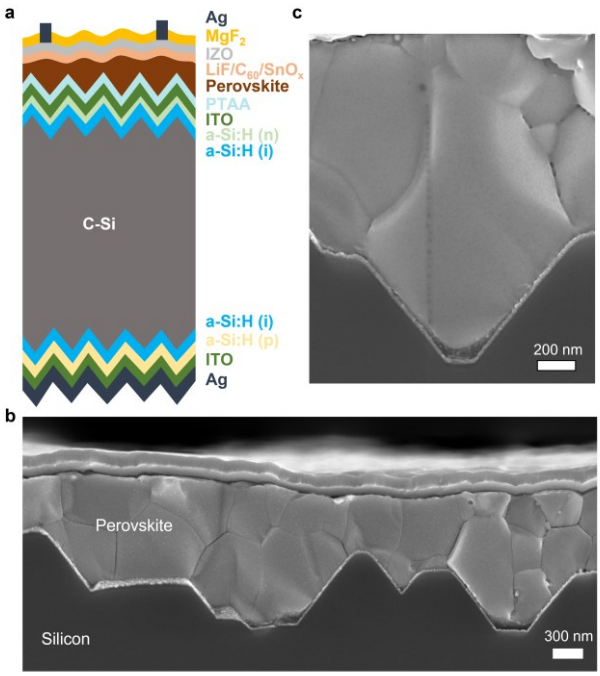

Figure 2. (a) Schematic of a perovskite/silicon tandem solar cell on a double-side-textured SHJ bottom cell. (b) Cross-sectional SEM image of a top perovskite cell on textured silicon bottom cells. (c) Cross-sectional SEM image of a spin-coated PTAA film in the valleys of a textured silicon wafer.

Recalling the enhanced conductivity of doped PTAA, we compared the performance of tandem cells using pristine PTAA, D-doped-PTAA, and LS-doped-PTAA doped with DPI-TPFB. Figure 3a plots the current-voltage (*J-V*) characteristics of the perovskite/silicon tandem devices under an aperture area of 1 cm^2 with three different PTAA HTLs, among which the PCEs are 25.0%, 25.8%, and 27.4%, respectively. The solar cell parameters for the three devices are summarized in Table 1. We observe a remarkable enhancement in FF, from approximately 73% to 79%, reaching that of perovskite/silicon tandem cells on surface-polished silicon subcells. The FF is also one of the highest reported for tandem cells fabricated on textured Si bottom cells (Figure S5 and Table S2). The high FF of the LS-doped PTAA device can be attributed to the improved conductivity made possible by the photoactivated p-doping of the thick HTL. Figure 3b displays the *J-V* characteristics under reverse and forward scans (which correspond to PCEs of 27.8% and 27.0%, respectively) of the champion perovskite/silicon device, in which the HTL is DPI-TPFB-doped PTAA formed under light. The detailed PV parameters of the champion device are listed in Table S2 and the statistics of PV parameters is shown in Figure 3f. The external quantum efficiency (EQE) spectra in Figure 3c indicate the integrated photocurrent densities, 19.7 mA/cm^2 for perovskite and 20.0 mA/cm^2 for silicon subcells, which are in agreement with the J_{SC} values from the *J-V* curve.

Table 1. Summary of photovoltaic parameters of the devices based on pristine, D-doped, and LS-doped PTAA as HTLs

HTLs	J_{SC} [mA/cm^2]	V_{OC} [V]	FF (%)	PCE (%)
Pristine PTAA	19.6	1.76	72.7	25.0
D-doped PTAA	19.5	1.75	75.4	25.8
LS-doped PTAA	19.49	1.79	79.1	27.4

The devices were encapsulated between two glass slides with butyl rubber as an edge sealant by a vacuum press laminator. To test the operational stability of the perovskite/silicon tandem cells, we held the target device at its maximum power point (MPP) under continuous xenon-lamp illumination for 200 hours and achieved stabilized device output with a negligible PCE drop, as shown in Figure 3d.

We also monitored the 5-week real-world stability of our encapsulated tandem devices outdoors in a hot and sunny desert climate, which is a targeted operational location for such efficient devices.[28, 38] The light intensity, measured by a pyranometer, varied from 0 at night to 0.9~1.2 sun at noon. Additionally, the high temperatures on the sunny days heated the device to well over 40°C. The daily light intensity and device performance are illustrated in Figure 3e. The PCE closely tracked the sun's light intensity (Figure S6). The initial PCE and the corresponding light intensity were 24.5 % and 0.81 sun, respectively. After over a month outdoors, the devices still yielded a PCE of 20.3% under 0.97 sun, which translates into a retention rate of 83% of the initial PCE over a month's period. Together, these device stability results provide evidence that the encapsulated perovskite/silicon tandem cells with doped PTAA possess a great tolerance to hot and sunny outdoor environments.

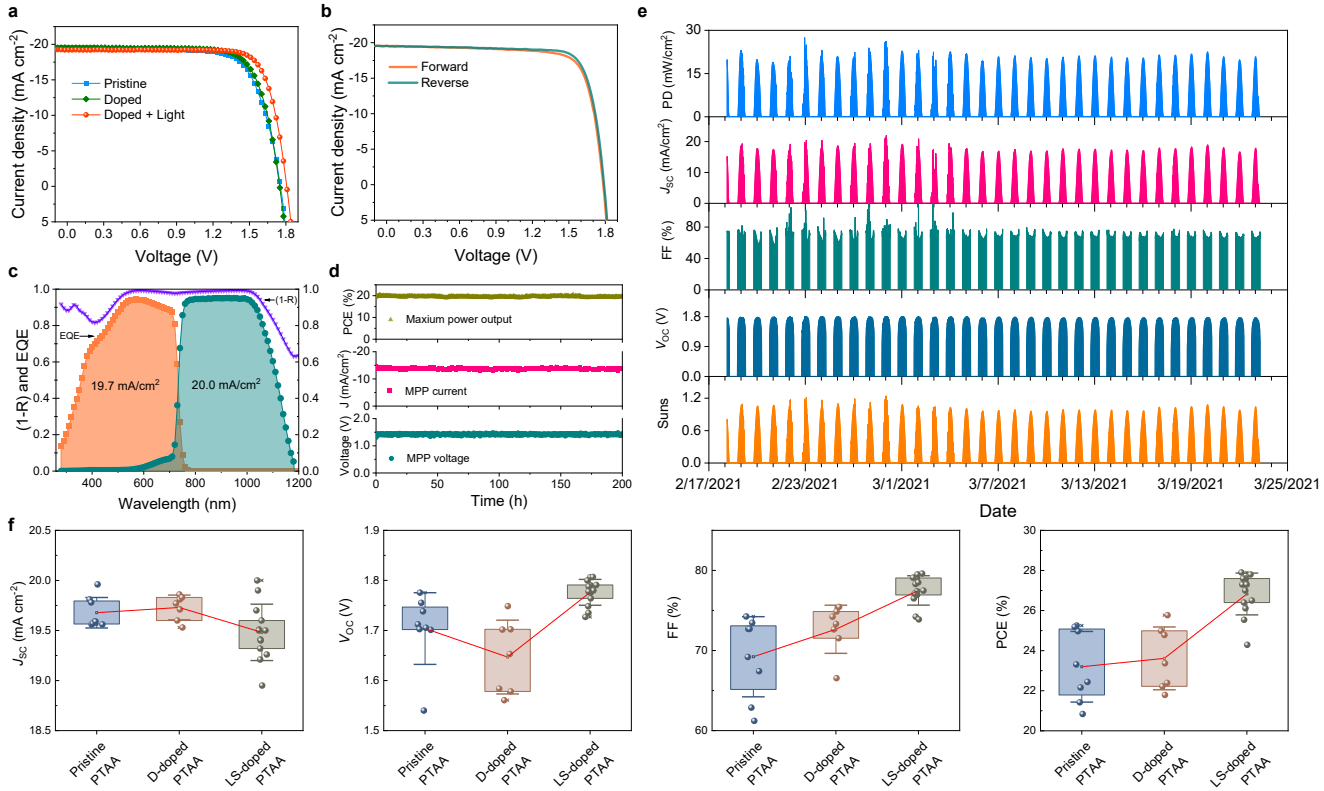

Figure 3. (a) *J-V* characteristics of perovskite/silicon tandem cells with pristine, D-doped, and LS-doped PTAA as HTLs. (b) Reverse- and forward-scanned *J-V* curves of the champion device containing LS-doped PTAA. (c) EQE spectrum of the target device. (d) Steady-state *J-V* output of the target cell at the MPP under simulated AM1.5G illumination. (e) Outdoor performance of the encapsulated target device in a hot desert climate, measured at the KAUST campus at Thuwal, Jeddah, Saudi Arabia from Feb 18th to Mar 23rd, 2021. PD, power density. (f) The PV parameters distribution of perovskite/silicon tandem devices.

In summary, we observe photoactivated p-type PTAA doping with DPI-TPFB, which greatly improve the conductivity of PTAA films. Films of the highly conductive PTAA material were applied to the textured silicon bottom cell of perovskite/silicon tandem cells, and a maximum FF of ~80%, which is comparable to the FF of perovskite/polished-silicon tandem cells, was achieved. Through the light-soaking treatment of DPI-TPFB-doped PTAA, perovskite/silicon tandem cells overcame the FF loss resulting from the non-uniform PTAA film on textured silicon, which boosted the PCE from 25.0% to 27.8%. This work provides a simple route to improving the hole transport properties of p-type organic materials and a feasible method for overcoming the deficient charge transport between textured silicon bottom subcells and perovskite top subcells.

ASSOCIATED CONTENT

Supporting Information

The Supporting Information is available free of charge on the ACS Publications website at

DOI: 10.XXX.

Materials and methods, UPS spectra of pristine, D-doped and LS-doped PTAA films, the PV characteristics of the typical silicon bottom cells, XRD patterns of the perovskite films, top-view SEM images of the perovskite films, reported fill factors of perovskite/silicon tandem cells, outdoor performance of the tandem device over a single day, resistance and conductivity of pristine and doped PTAA, forward and reverse scans for the champion cell with an LS-doped PTAA HTL.

AUTHOR INFORMATION

Corresponding Author

*omar.abdelsaboor@kaust.edu.sa

*stefaan.dewolf@kaust.edu.sa

*osman.bakr@kaust.edu.sa

Author Contributions

‖These authors contributed equally.

Notes

The authors declare no competing financial interests.

ACKNOWLEDGMENT

The authors acknowledge the funding support from KAUST and Aramco (grant no. RGC/3/4556-01-01). J.L., E.A., M.D.B., and S.D.W., thanks to KAUST for funding under the Award No. OSR-CARF/CCF-3079, OSR-CRG2019-4093, and IED OSR-2019-4208. This work was authored in part by the National Renewable Energy Laboratory, operated by Alliance for Sustainable Energy, LLC, for the U.S. Department of Energy (DOE) under Contract No. DE-AC36-08GO28308. The NREL affiliated authors acknowledge the Tandem Photovoltaics project funded by the Solar Energy Technology Office within the US DOE Energy Efficiency and Renewable Energy under contract SETP DE- EE00038266. T.L., K.N.B., and K.R.G. acknowledge funding from the National Science Foundation under award OIA-1929131 (T.L. and K.R.G) and DMR-1905734 (K.N.B. and K.R.G).The views expressed in the article do not necessarily represent the views of the DOE or the U.S. Government.

REFERENCES

1. Kojima, A.; Teshima, K.; Shirai, Y.; Miyasaka, T., Organometal Halide Perovskites as Visible-Light Sensitizers for Photovoltaic Cells. *J. Am. Chem. Soc.* **2009,** *131* (17), 6050-6051.
2. Lee, M. M.; Teuscher, J.; Miyasaka, T.; Murakami, T. N.; Snaith, H. J., Efficient Hybrid Solar Cells Based on Meso-Superstructured Organometal Halide Perovskites. *Science* **2012,** *338* (6107), 643.
3. Kim, H.-S.; Lee, C.-R.; Im, J.-H.; Lee, K.-B.; Moehl, T.; Marchioro, A.; Moon, S.-J.; Humphry-Baker, R.; Yum, J.-H.; Moser, J. E.; Grätzel, M.; Park, N.-G., Lead Iodide Perovskite Sensitized All-Solid-State Submicron Thin Film Mesoscopic Solar Cell with Efficiency Exceeding 9%. *Sci. Rep.* **2012,** *2* (1), 591.
4. Min, H.; Lee, D. Y.; Kim, J.; Kim, G.; Lee, K. S.; Kim, J.; Paik, M. J.; Kim, Y. K.; Kim, K. S.; Kim, M. G.; Shin, T. J.; Il Seok, S., Perovskite solar cells with atomically coherent interlayers on SnO_2 electrodes. *Nature* **2021,** *598* (7881), 444-450.
5. Shi, D.; Adinolfi, V.; Comin, R.; Yuan, M.; Alarousu, E.; Buin, A.; Chen, Y.; Hoogland, S.; Rothenberger, A.; Katsiev, K.; Losovyj, Y.; Zhang, X.; Dowben Peter, A.; Mohammed Omar, F.; Sargent Edward, H.; Bakr Osman, M., Low trap-state density and long carrier diffusion in organolead trihalide perovskite single crystals. *Science* **2015,** *347* (6221), 519-522.
6. Turedi, B.; Yeddu, V.; Zheng, X.; Kim, D. Y.; Bakr, O. M.; Saidaminov, M. I., Perovskite Single-Crystal Solar Cells: Going Forward. *ACS Energy Lett.* **2021,** *6* (2), 631-642.
7. Zheng, X.; Troughton, J.; Gasparini, N.; Lin, Y.; Wei, M.; Hou, Y.; Liu, J.; Song, K.; Chen, Z.; Yang, C.; Turedi, B.; Alsalloum, A. Y.; Pan, J.; Chen, J.; Zhumekenov, A. A.; Anthopoulos, T. D.; Han, Y.; Baran, D.; Mohammed, O. F.; Sargent, E. H.; Bakr, O. M., Quantum Dots Supply Bulk- and Surface-Passivation Agents for Efficient and Stable Perovskite Solar Cells. *Joule* **2019,** *3* (8), 1963-1976.

8. Best Research-Cell Efficiency Chart. National Renewable Energy Laboratory. https://www.nrel.gov/pv/cell-efficiency.html (accessed Apr 26, 2022).
9. Zheng, X.; Hou, Y.; Bao, C.; Yin, J.; Yuan, F.; Huang, Z.; Song, K.; Liu, J.; Troughton, J.; Gasparini, N.; Zhou, C.; Lin, Y.; Xue, D.-J.; Chen, B.; Johnston, A. K.; Wei, N.; Hedhili, M. N.; Wei, M.; Alsalloum, A. Y.; Maity, P.; Turedi, B.; Yang, C.; Baran, D.; Anthopoulos, T. D.; Han, Y.; Lu, Z.-H.; Mohammed, O. F.; Gao, F.; Sargent, E. H.; Bakr, O. M., Managing grains and interfaces via ligand anchoring enables 22.3%-efficiency inverted perovskite solar cells. *Nat. Energy* **2020,** *5* (2), 131-140.
10. Alsalloum, A. Y.; Turedi, B.; Almasabi, K.; Zheng, X.; Naphade, R.; Stranks, S. D.; Mohammed, O. F.; Bakr, O. M., 22.8%-Efficient single-crystal mixed-cation inverted perovskite solar cells with a near-optimal bandgap. *Energy Environ. Sci.* **2021,** *14* (4), 2263-2268.
11. Alsalloum, A. Y.; Turedi, B.; Zheng, X.; Mitra, S.; Zhumekenov, A. A.; Lee, K. J.; Maity, P.; Gereige, I.; AlSaggaf, A.; Roqan, I. S.; Mohammed, O. F.; Bakr, O. M., Low-Temperature Crystallization Enables 21.9% Efficient Single-Crystal $MAPbI_3$ Inverted Perovskite Solar Cells. *ACS Energy Lett.* **2020,** *5* (2), 657-662.
12. Yu, Z.; Leilaeioun, M.; Holman, Z., Selecting tandem partners for silicon solar cells. *Nat. Energy* **2016,** *1* (11), 16137.
13. Hou, Y.; Aydin, E.; De Bastiani, M.; Xiao, C.; Isikgor Furkan, H.; Xue, D.-J.; Chen, B.; Chen, H.; Bahrami, B.; Chowdhury Ashraful, H.; Johnston, A.; Baek, S.-W.; Huang, Z.; Wei, M.; Dong, Y.; Troughton, J.; Jalmood, R.; Mirabelli Alessandro, J.; Allen Thomas, G.; Van Kerschaver, E.; Saidaminov Makhsud, I.; Baran, D.; Qiao, Q.; Zhu, K.; De Wolf, S.; Sargent Edward, H., Efficient tandem solar cells with solution-processed perovskite on textured crystalline silicon. *Science* **2020,** *367* (6482), 1135-1140.
14. Liu, J.; Aydin, E.; Yin, J.; De Bastiani, M.; Isikgor, F. H.; Rehman, A. U.; Yengel, E.; Ugur, E.; Harrison, G. T.; Wang, M.; Gao, Y.; Khan, J. I.; Babics, M.; Allen, T. G.; Subbiah, A. S.; Zhu, K.; Zheng, X.; Yan, W.; Xu, F.; Salvador, M. F.; Bakr, O. M.; Anthopoulos, T. D.; Lanza, M.; Mohammed, O. F.; Laquai, F.; De Wolf, S., 28.2%-efficient, outdoor-stable perovskite/silicon tandem solar cell. *Joule* **2021,** *5* (12), 3169-3186.
15. Han, Q.; Hsieh, Y.-T.; Meng, L.; Wu, J.-L.; Sun, P.; Yao, E.-P.; Chang, S.-Y.; Bae, S.-H.; Kato, T.; Bermudez, V.; Yang, Y., High-performance perovskite/Cu(In,Ga)Se_2 monolithic tandem solar cells. *Science* **2018,** *361* (6405), 904-908.
16. Al-Ashouri, A.; Köhnen, E.; Li, B.; Magomedov, A.; Hempel, H.; Caprioglio, P.; Márquez José, A.; Morales Vilches Anna, B.; Kasparavicius, E.; Smith Joel, A.; Phung, N.; Menzel, D.; Grischek, M.; Kegelmann, L.; Skroblin, D.; Gollwitzer, C.; Malinauskas, T.; Jošt, M.; Matič, G.; Rech, B.; Schlatmann, R.; Topič, M.; Korte, L.; Abate, A.; Stannowski, B.; Neher, D.; Stolterfoht, M.; Unold, T.; Getautis, V.; Albrecht, S., Monolithic perovskite/silicon tandem solar cell with >29% efficiency by enhanced hole extraction. *Science* **2020,** *370* (6522), 1300-1309.
17. Chen, B.; Yu, Z.; Liu, K.; Zheng, X.; Liu, Y.; Shi, J.; Spronk, D.; Rudd, P. N.; Holman, Z.; Huang, J., Grain Engineering for Perovskite/Silicon Monolithic Tandem Solar Cells with Efficiency of 25.4%. *Joule* **2019,** *3* (1), 177-190.
18. Kim, D.; Jung Hee, J.; Park Ik, J.; Larson Bryon, W.; Dunfield Sean, P.; Xiao, C.; Kim, J.; Tong, J.; Boonmongkolras, P.; Ji Su, G.; Zhang, F.; Pae Seong, R.; Kim, M.; Kang Seok, B.; Dravid, V.; Berry Joseph, J.; Kim Jin, Y.; Zhu, K.; Kim Dong, H.; Shin, B., Efficient, stable silicon tandem cells enabled by anion-engineered wide-bandgap perovskites. *Science* **2020,** *368* (6487), 155-160.
19. Xu, J.; Boyd Caleb, C.; Yu Zhengshan, J.; Palmstrom Axel, F.; Witter Daniel, J.; Larson Bryon, W.; France Ryan, M.; Werner, J.; Harvey Steven, P.; Wolf Eli, J.; Weigand, W.; Manzoor, S.; van Hest Maikel, F. A. M.; Berry Joseph, J.; Luther Joseph, M.; Holman Zachary, C.; McGehee Michael, D., Triple-halide wide–band gap perovskites with suppressed phase segregation for efficient tandems. *Science* **2020,** *367* (6482), 1097-1104.
20. Zheng, X.; Alsalloum, A. Y.; Hou, Y.; Sargent, E. H.; Bakr, O. M., All-Perovskite Tandem Solar Cells: A Roadmap to Uniting High Efficiency with High Stability. *Acc. Mater. Res.* **2020,** *1* (1), 63-76.
21. Jošt, M.; Köhnen, E.; Al-Ashouri, A.; Bertram, T.; Tomšič, Š.; Magomedov, A.; Kasparavicius, E.; Kodalle, T.; Lipovšek, B.; Getautis, V.; Schlatmann, R.; Kaufmann, C. A.; Albrecht, S.; Topič, M., Perovskite/CIGS Tandem Solar Cells: From Certified 24.2% toward 30% and Beyond. *ACS Energy Lett.* **2022,** *7* (4), 1298-1307.
22. Li, W.; Zheng, J.; Hu, B.; Fu, H.-C.; Hu, M.; Veyssal, A.; Zhao, Y.; He, J.-H.; Liu, T. L.; Ho-Baillie, A.; Jin, S., High-performance solar flow battery powered by a perovskite/silicon tandem solar cell. *Nat. Mater.* **2020,** *19* (12), 1326-1331.
23. Jošt, M.; Bertram, T.; Koushik, D.; Marquez, J. A.; Verheijen, M. A.; Heinemann, M. D.; Köhnen, E.; Al-Ashouri, A.; Braunger, S.; Lang, F.; Rech, B.; Unold, T.; Creatore, M.; Lauermann, I.; Kaufmann, C. A.; Schlatmann, R.; Albrecht, S., 21.6%-Efficient Monolithic Perovskite/Cu(In,Ga)Se_2 Tandem Solar Cells with Thin Conformal Hole Transport Layers for Integration on Rough Bottom Cell Surfaces. *ACS Energy Lett.* **2019,** *4* (2), 583-590.
24. Zheng, J.; Mehrvarz, H.; Liao, C.; Bing, J.; Cui, X.; Li, Y.; Gonçales, V. R.; Lau, C. F. J.; Lee, D. S.; Li, Y.; Zhang, M.; Kim, J.; Cho, Y.; Caro, L. G.; Tang, S.; Chen, C.; Huang, S.; Ho-Baillie, A. W. Y., Large-Area 23%-Efficient Monolithic Perovskite/Homojunction-Silicon Tandem Solar Cell with Enhanced UV Stability Using Down-Shifting Material. *ACS Energy Lett.* **2019,** *4* (11), 2623-2631.
25. Bush, K. A.; Palmstrom, A. F.; Yu, Z. J.; Boccard, M.; Cheacharoen, R.; Mailoa, J. P.; McMeekin, D. P.; Hoye, R. L. Z.; Bailie, C. D.; Leijtens, T.; Peters, I. M.; Minichetti, M. C.; Rolston, N.; Prasanna, R.; Sofia, S.; Harwood, D.; Ma, W.; Moghadam, F.; Snaith, H. J.; Buonassisi, T.; Holman, Z. C.; Bent, S. F.; McGehee, M. D., 23.6%-efficient monolithic perovskite/silicon tandem solar cells with improved stability. *Nat. Energy* **2017,** *2* (4), 17009.
26. Bush, K. A.; Manzoor, S.; Frohna, K.; Yu, Z. J.; Raiford, J. A.; Palmstrom, A. F.; Wang, H.-P.; Prasanna, R.; Bent, S. F.; Holman, Z. C.; McGehee, M. D., Minimizing Current and Voltage Losses to Reach 25% Efficient Monolithic Two-Terminal Perovskite–Silicon Tandem Solar Cells. *ACS Energy Lett.* **2018,** *3* (9), 2173-2180.
27. Sahli, F.; Werner, J.; Kamino, B. A.; Bräuninger, M.; Monnard, R.; Paviet-Salomon, B.; Barraud, L.; Ding, L.; Diaz Leon, J. J.; Sacchetto, D.; Cattaneo, G.; Despeisse, M.; Boccard, M.; Nicolay, S.; Jeangros, Q.; Niesen, B.; Ballif, C., Fully textured monolithic perovskite/silicon tandem solar cells with 25.2% power conversion efficiency. *Nat. Mater.* **2018,** *17* (9), 820-826.
28. Aydin, E.; Allen, T. G.; De Bastiani, M.; Xu, L.; Ávila, J.; Salvador, M.; Van Kerschaver, E.; De Wolf, S., Interplay between temperature and bandgap energies on the outdoor performance of perovskite/silicon tandem solar cells. *Nat. Energy* **2020,** *5* (11), 851-859.

29. Chen, B.; Yu, Z. J.; Manzoor, S.; Wang, S.; Weigand, W.; Yu, Z.; Yang, G.; Ni, Z.; Dai, X.; Holman, Z. C.; Huang, J., Blade-Coated Perovskites on Textured Silicon for 26%-Efficient Monolithic Perovskite/Silicon Tandem Solar Cells. *Joule* **2020,** *4* (4), 850-864.
30. Tennyson, E. M.; Frohna, K.; Drake, W. K.; Sahli, F.; Chien-Jen Yang, T.; Fu, F.; Werner, J.; Chosy, C.; Bowman, A. R.; Doherty, T. A. S.; Jeangros, Q.; Ballif, C.; Stranks, S. D., Multimodal Microscale Imaging of Textured Perovskite–Silicon Tandem Solar Cells. *ACS Energy Lett.* **2021,** *6* (6), 2293-2304.
31. Nogay, G.; Sahli, F.; Werner, J.; Monnard, R.; Boccard, M.; Despeisse, M.; Haug, F. J.; Jeangros, Q.; Ingenito, A.; Ballif, C., 25.1%-Efficient Monolithic Perovskite/Silicon Tandem Solar Cell Based on a p-type Monocrystalline Textured Silicon Wafer and High-Temperature Passivating Contacts. *ACS Energy Lett.* **2019,** *4* (4), 844-845.
32. Baker-Finch, S. C.; McIntosh, K. R., Reflection of normally incident light from silicon solar cells with pyramidal texture. *Prog. Photovoltaics* **2011,** *19* (4), 406-416.
33. Ke, W.; Stoumpos, C. C.; Spanopoulos, I.; Mao, L.; Chen, M.; Wasielewski, M. R.; Kanatzidis, M. G., Efficient Lead-Free Solar Cells Based on Hollow {en}$MASnI_3$ Perovskites. *J. Am. Chem. Soc.* **2017,** *139* (41), 14800-14806.
34. Ye, T.; Chen, W.; Jin, S.; Hao, S.; Zhang, X.; Liu, H.; He, D., Enhanced Efficiency of Planar Heterojunction Perovskite Solar Cells by a Light Soaking Treatment on Tris(pentafluorophenyl)borane-Doped Poly(triarylamine) Solution. *ACS Appl. Mater. Interfaces* **2019,** *11* (15), 14004-14010.
35. Liang, Z.; Choi, H. H.; Luo, X.; Liu, T.; Abtahi, A.; Ramasamy, U. S.; Hitron, J. A.; Baustert, K. N.; Hempel, J. L.; Boehm, A. M.; Ansary, A.; Strachan, D. R.; Mei, J.; Risko, C.; Podzorov, V.; Graham, K. R., n-type charge transport in heavily p-doped polymers. *Nat. Mater.* **2021,** *20* (4), 518-524.
36. Dektar, J. L.; Hacker, N. P., Photochemistry of diaryliodonium salts. *J. Org. Chem.* **1990,** *55* (2), 639-647.
37. Seim, H.; Haase, N.; Scheible, K.; Heil, H.; Böhm, E.; Buchholz, H.; von Seggern, H., Photoactivation of an ionic p-type dopant used in a triarylamine based hole transporting material for enhancing conductivity of solution processed films. *Synth. Met.* **2017,** *230*, 105-112.
38. De Bastiani, M.; Van Kerschaver, E.; Jeangros, Q.; Ur Rehman, A.; Aydin, E.; Isikgor, F. H.; Mirabelli, A. J.; Babics, M.; Liu, J.; Zhumagali, S.; Ugur, E.; Harrison, G. T.; Allen, T. G.; Chen, B.; Hou, Y.; Shikin, S.; Sargent, E. H.; Ballif, C.; Salvador, M.; De Wolf, S., Toward Stable Monolithic Perovskite/Silicon Tandem Photovoltaics: A Six-Month Outdoor Performance Study in a Hot and Humid Climate. *ACS Energy Lett.* **2021,** *6* (8), 2944-2951.
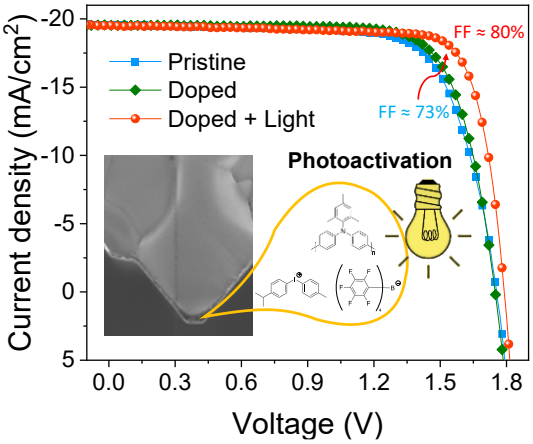
Table of content